Electrical Behavior of SnO_2 Polycrystalline Ceramic Pieces Formed by Slip Casting: Effect of Surrounding Atmosphere (Air and CO)

C. J. Aguilar-Paz, Y. Ochoa-Muñoz, M. A. Ponce & J. E. Rodríguez-Páez

Journal of Electronic Materials

ISSN 0361-5235

Journal of Elec Materi
DOI 10.1007/s11664-015-4153-2

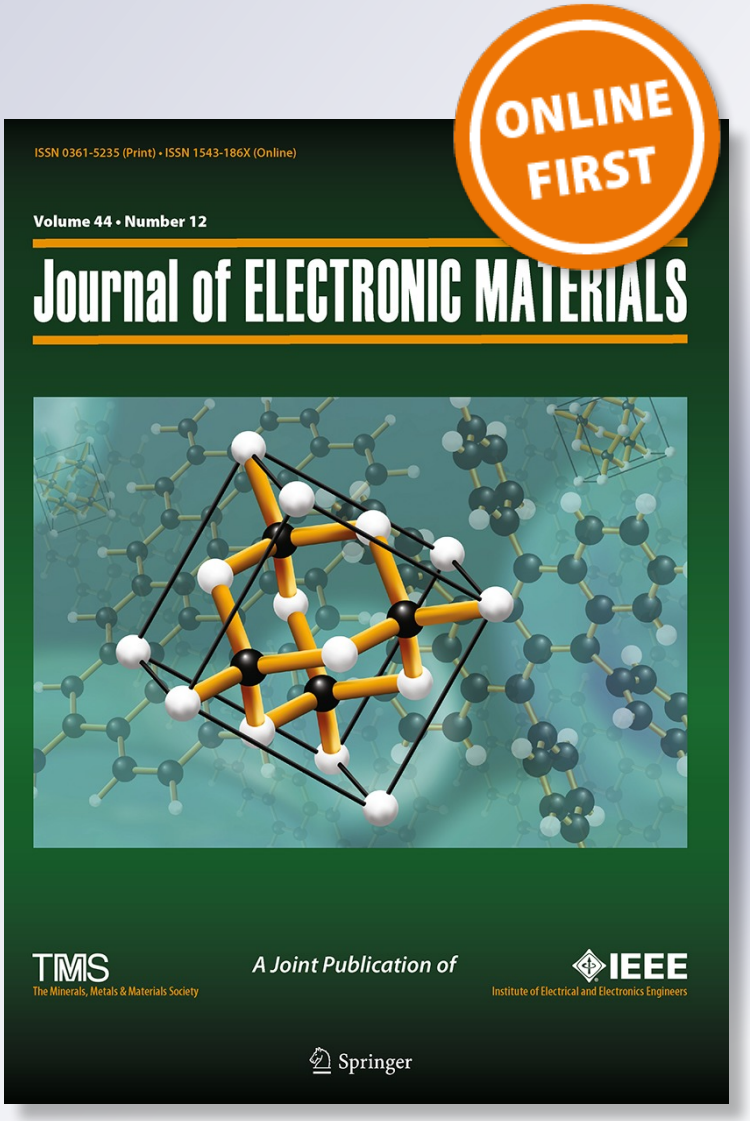

Springer

Your article is protected by copyright and all rights are held exclusively by The Minerals, Metals & Materials Society. This e-offprint is for personal use only and shall not be self-archived in electronic repositories. If you wish to self-archive your article, please use the accepted manuscript version for posting on your own website. You may further deposit the accepted manuscript version in any repository, provided it is only made publicly available 12 months after official publication or later and provided acknowledgement is given to the original source of publication and a link is inserted to the published article on Springer's website. The link must be accompanied by the following text: "The final publication is available at link.springer.com".

Author's personal copy

Journal of ELECTRONIC MATERIALS
DOI: 10.1007/s11664-015-4153-2
© 2015 The Minerals, Metals & Materials Society

Electrical Behavior of SnO_2 Polycrystalline Ceramic Pieces Formed by Slip Casting: Effect of Surrounding Atmosphere (Air and CO)

C.J. AGUILAR-PAZ,[1] Y. OCHOA-MUÑOZ,[1,3] M.A. PONCE,[2] and J.E. RODRÍGUEZ-PÁEZ[1]

1.—CYTEMAC Group – Department of Physics, University of Cauca, Popayán, Colombia. 2.—Institute of Science and Technology of Materials (INTEMA), National University of Mar del Plata, National Research Council (CONICET), Juan B. Justo 4302, B7608FDQ Mar del Plata, Argentina. 3.—e-mail: yochoa@unicauca.edu.co

Pieces of porous polycrystalline SnO_2 with and without cobalt have been formed by the slip-casting method, using ceramic powders synthesized by the controlled precipitation method. A suitable methodology was developed for forming and sintering the pieces to enable controlled modification of their microstructure, principally grain size, porosity, and type of intergranular contacts. Better control of the microstructure was obtained in the samples containing cobalt. In these, predominance of open necks and intergranular contacts was observed, which can represent Schottky barriers. Because of its good structural homogeneity, porosity, and small grain size (of the order of 1 μm), the sample with 2 mol.% Co sintered at 1250°C for 2 h was selected for electrical characterization by complex impedance spectroscopy, varying the operating temperature, concentration and nature of the surrounding gas (air or CO), and bias voltage. The resulting R_p and C_p curves were very sensitive to variation in these parameters, being most obvious for the C_p curves, which showed a phenomenon of low-frequency dispersion when bias voltages other than zero were used, in the presence of O_2, and at operating temperature of 280°C. The electrical behavior of the SnO_2 with 2 mol.% Co sample sintered at 1250°C was consistent with the nature and microstructural characteristics of the active material and was justified based on the presence of shallow- and deep-type defects, and variations in barrier height and width, caused by adsorption of gas molecules.

Key words: Synthesis, slip casting, electrical characterization, gas sensing

INTRODUCTION

Since the demonstration 60 years ago that gas adsorption onto a semiconductor surface can significantly change its electrical resistance,[1,2] work on the use of this phenomenon for gas detection has made significant progress.[3–5] Although initial studies were performed with ZnO, other oxides have also been used, including TiO_2, WO_2, CeO_2, and particularly SnO_2 due to its high sensitivity at low operating temperature.[6–8] As the surface characteristics and properties of these active materials are extremely important, achieving a high surface-to-bulk ratio is crucial in device manufacture. This has been achieved to some degree by designing commercial devices in the form of thin films or highly porous pieces, with loosely sintered particles,[9] or nanostructured materials.[6]

Sensors formed using porous materials and containing precious metals as catalysts have shown a high degree of sensitivity to the presence of gases, also offering the advantages of light weight and simple, low-cost manufacturing processes.[9,10] The

(Received May 23, 2015; accepted October 13, 2015)

Published online: 06 November 2015

Author's personal copy

main disadvantage of such porous active materials is their relative lack of selectivity, yielding a response to most reducing gases.[9] To improve the selectivity and reduce the high power consumption during sensor operation, it is necessary to improve understanding of how these porous materials work for gas sensing. Specifically, the conduction model used to justify and explain the behavior of the material in the presence of a certain gas should consider that the conductivity in the solid can be controlled by different types of intergranular contacts, represented by necks or bridges, necks depleted of conduction electrons, and Schottky barriers.[9–14] These structural inhomogeneities generate conduction paths with lower resistance along the grains, alternating with areas of high resistance at the contact points.

In this model of electrical conduction for gas sensors with porous structure, it is necessary to consider the characteristics of the intergranular contacts, in particular the extension of the depletion layer, which affects the contribution of the intergranular zones to the overall conductivity.[9,10,15] Figure 1 shows the most general types of intergranular zones involving open (Fig. 1a) or closed (Fig. 1b) necks or bridges and the presence of Schottky-type barriers (Fig. 1c). In the case of fully open necks (Fig. 1a), the surface states generate a depletion zone that extends to a certain depth, indicated by the shaded region on both sides of the neck, leaving a zone in the center of the bridge through which the conductivity should be greater. In this case, the depletion zones do not overlap and therefore no barriers to carrier movement are formed, so the conductivity is determined by electron activation from donor states in the bulk (being limited by trap defects in the bulk), a process that can be affected by the gas atmosphere.[9] When open bridges predominate in such porous active material or there are sufficient continuous paths containing only bridges of this type in the interior, the presence of dopants in the solid becomes important.[9,10,15,16] In this case, both gas adsorption and other effects external to the sensor may change the surface charge, altering the width of the depletion layer and thus the thickness of the conducting channel, modifying the electrical resistivity of the neck.

In the case of closed necks or bridges (Fig. 1b), the depletion zones from two surfaces overlap, creating a conduction path with high ohmic resistance in the center of the neck. For closed bridges, it is possible that high energy barriers may be formed (with height greater than kT) due to the overlapping depletion regions when the neck size is small ($h < 2L_D$, where h is the size of the neck and L_D is the shielding Debye length), and a large amount of surface charge is accumulated. This geometry can be generated during the early stages of sintering the material or when, in an open bridge, the thickness of the depletion layer is altered. In closed bridges, the conduction is determined by electron activation from surface states toward the conduction band (a process limited by surface traps), and this may be affected by the occupation of the surface states due to adsorption of the surrounding gas. In the case of active materials in which the total resistivity of the sample is controlled by closed necks, the greatest drop in the external applied voltage occurs in these bridges and the change in the value of the surface charge which would cause the greatest variation in the electrical conductivity of the active material. Therefore, variations in conditions external to the material, such as adsorption, temperature, and illumination, can affect the surface charge and thereby the conductivity of the material.[15]

For the case where necks or bridges, either open or closed, are the significant intergranular contacts and determine the conductivity of the sensor, parameters such as the size of the necks, the degree of doping of the material or the defect concentration in these zones, and the value of the localized surface charge on the surface states may affect the movement of charge carriers in the semiconductor.[10] Previous studies showed that the conductivity can be controlled by bulk or surface traps depending on the oxygen pressure or combustible gas concentration.[17]

In the third type of intergranular zone (Fig. 1c), the contacts between the grains can be represented by Schottky-type barriers formed outside the charge trapped in the surface states. In this case, the conductivity is controlled by the transport of charge through the barrier, so the activation energy will be directly affected by the charge and the coverage by surface species, in other words by the fractional coverage of these species and their composition. Specifically, for these contacts where isotype heterotransitions occur, the electrical conductivity of the material will depend on the height and width of the intergranular barriers, which can be affected by, among other external factors, adsorption of gases.[14,18–23] Each of the three types of intergranular contact illustrated in Fig. 1 contains a grain boundary at which trap states can establish a depletion layer. If the grain size is small enough, it might be depleted of conduction electrons, thereby facilitating limited conductivity by way of excitation from the traps of the grain boundary.[24]

Determining the effect of an active material's microstructure on its sensing capability has been a subject of great interest, since if the dependence of the conductivity of the material is determined by the porosity of the sintered part, the working temperature, and the nature of the gas, the electrical characteristics of the porous active material can be optimized.[4,6,9–14,25] Numerous studies are needed to model the pore structure of the active material and relate it to the sensor behavior that it shows. This information is invaluable in the case of highly porous structures that are normally obtained by using nanoparticles, exhibiting high surface-to-volume ratio and therefore high sensitivity to gases due to

Author's personal copy

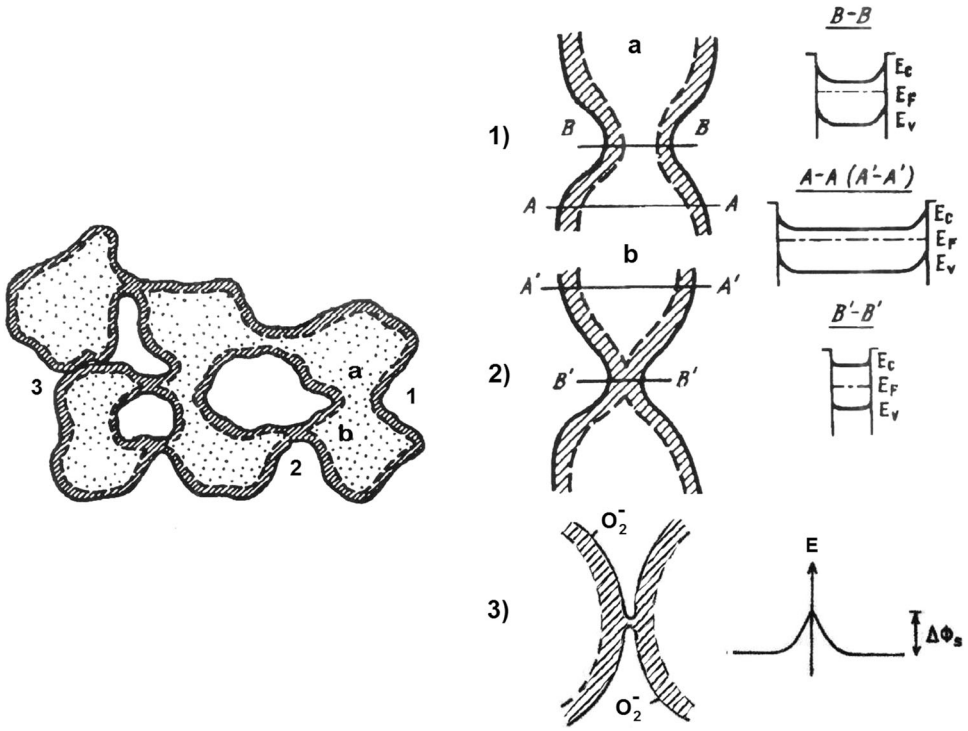

Fig. 1. The most general types of intergranular contact present in the microstructure of porous polycrystalline material: (1) open necks or bridges, (2) closed necks or bridges, and (3) contacts that can be represented by Schottky-type barriers.

the role played by gas–surface interactions in the detection process.[6,26] Jones et al.[27] studied the electrical response of three physical forms of zinc oxide—monocrystal, polycrystal, and pressed discs—in the presence of CH_4, CO, and H_2O. The study conducted by these researchers on oxygen adsorption and desorption showed that the corresponding photoadsorption and photodesorption processes differ substantially depending on the type of sample used. Specifically, the nature and concentration of defects, such as high concentration of superstoichiometric zinc on the surface and in adjacent layers, enable understanding of these behavioral differences between samples to some degree.

Willett et al.[28] investigated the correlation between the gas sensing properties of SnO_2 pieces sintered at different temperatures and the pore structure of the samples. Specifically, they correlated the nature of the pore structure present in nanostructured SnO_2 materials with their sensing properties and found evidence of a direct relationship between porosity and gas sensitivity, for samples that did not experience significant grain growth, such that, under fixed operating conditions, the pore structure strongly affected the sensitivity of the samples. For material sintered at temperatures below 1200°C, the sensitivity to gas depended strongly on temperature and, when the grain growth was low, on the diffusion of the gas inside the porous oxide structure. For materials sintered at higher temperatures, with large pore structure, the dominant process was surface reactions.

Ahn et al.[29] studied the effects of microstructural changes after sintering at different temperatures on the hydrogen sensing properties of thick films formed using SnO_2 powders. The films were formed by silk-screen printing and subsequently treated at different temperatures between 50°C and 900°C for 1 h in air. The films sintered at 600°C and applied at a working temperature of 250°C showed the highest sensitivity. For these researchers, the crystallinity of the thick film was an important parameter to account for the sensitivity to the presence of gases, as it would control the concentration of intrinsic defects in the tin oxide.

Therefore, to optimize the sensitivity of the active material, the growth of necks or bridges between grains should be controlled and minimized, and the crystallinity of the material improved. In actual porous materials, all three kinds of intergranular contact may be found (Fig. 1). If predominance of one of these is desired so that a given conductivity mechanism is favored as described above, the manufacturing processes and subsequent treatment applied to the sample must be controlled. Specifically, it is necessary to research the contradictory effects of sintering temperature systematically, since it affects both the microstructure and crystallinity of the active material and thereby its electrical behavior. One technique for forming ceramic pieces that can be used to control the predominance of a particular type of intergranular contact is the colloidal or slip-casting method.[30,31] When using this method based on the formation of stable slip, a

Author's personal copy

number of parameters can be controlled, such as the solids percentage in the slurry, the type of additives used, the dopants (for control over diffusional processes, for example), and the size and morphology of the particles of the raw material, among others. Following the formation of a green part, the sinterability of the porous material can be adjusted to favor a particular type of intergranular contact, by considering what happens in the different stages of sintering as already widely studied.[32,33]

In this work, pieces of SnO_2 ceramic with and without Co were formed using the slip-casting method. These pieces were sintered at different temperatures to modify their microstructure, mainly in terms of the porosity, grain size, and type of intergranular contacts. Cobalt was used as a dopant to promote the sinterability of the SnO_2 pieces through generation of oxygen vacancies as a result of local charge imbalance resulting from substitution of Sn^{4+} by Co^{2+}. By controlling the percentage of Co incorporated into the material, a given concentration of extrinsic defects can be established. From among the sintered samples, that which presented the most homogeneous structure in terms of porosity was selected and characterized electrically by complex impedance spectroscopy in the presence of air or CO atmosphere, at different working temperatures, and under different bias voltages.

EXPERIMENTAL PROCEDURES

Obtaining SnO_2 Powders with and Without Doping by the Controlled Precipitation Method

To synthesize cassiterite-phase tin oxide SnO_2, an aqueous solution was prepared with 1 M $SnCl_2{\cdot}2H_2O$ tin precursor (99.6%; Mallinckrodt) and 0.1 M HNO_3 (99%; Carlo Erba). The solution was stirred constantly at 200 rpm at room temperature until no precursor particles were observed either in suspension or as sediment. Then, ammonium hydroxide (NH_4OH, 28%; Mallincrodt) was added at rate of 0.034 mL/s using a dispenser (685 Metrohm Dosimat). The variation in the pH of the system was recorded using a pH meter (Metrohm 744) with a glass electrode, and the specific conductivity of the system was measured using a conductivity meter (Toledo model MC126).

As NH_4OH was added to the system, the pH and specific conductivity were recorded to plot potentiometric and conductometric titration curves for the tin system as a function of the volume of NH_4OH precipitant added, in order to choose the most suitable pH value for synthesis of tin oxide. Based on the results of this and previous studies,[34] a working pH of 4.2 was chosen. The obtained suspension was filtered in vacuum to remove solvent using a Buchi B-169 pump, allowing separation of the solid and liquid phases; the filtrate was obtained as a wet gel.

In this paper, "washing process" is used to refer to redispersion of the obtained colloidal suspension, after filtration, in a solvent such as water or alcohol, a process performed primarily to remove impurities or chemical species, for example, anions accompanying Sn in the precursor. To carry out the washing, an aqueous solution of diethylamine (Merck) was used at concentration of 0.05 M. The precipitate was redispersed in this solution using a high-shear dispersion device (Ultraturrax IKA model T-50), subjecting the mixture to stirring speed of 4000 rpm for 3 min; the final gel obtained was left to age for 24 h.

The resulting colloidal suspension was filtered and redispersed again in the solution with diethylamine, once more leaving it to age for 24 h. This process was repeated four times. The wet solid, the filtrate end product, was dried in an oven at 60°C for 24 h, then macerated in an agate mortar; the obtained powder was then characterized. In conclusion, the most suitable conditions for SnO_2 synthesis by precipitation were pH 4.2 in aqueous solution with 1 M concentration of tin precursor ($SnCl_2{\cdot}2H_2O$) and 0.1 M HNO_3, plus aging of the precipitate in the mother solution for 15 days followed by washing four times using 0.05 M diethylamine solution.

To obtain cobalt-doped SnO_2 powders, aqueous suspensions of tin and cobalt were prepared separately. The tin suspension was obtained as described above. The cobalt precipitate was prepared using suitable amounts of cobalt acetate (99.6%; Mallinckrodt) to achieve Co concentrations of 0.5 mol.%, 1 mol.%, and 2 mol.% in the system. Table I presents the doping percentages and nomenclature used for the SnO_2–CoO system in this work.

To obtain the precipitate of Co, cobalt acetate solution was initially used, with NH_4OH as precipitating agent. Based on the results of potentiometric titration as described above, it was determined that the optimum pH to obtain the precipitate was 6. Subsequently, the suspensions of tin and cobalt were mixed, without any treatment; the obtained system was redispersed using the high-shear stirrer, and the resulting suspension was subjected to repeated washing procedures using 0.05 M aqueous solution of diethylamine. The wet solid obtained at the end of this process was dried and pulverized in an agate mortar, and the obtained powder was subjected to heat treatment at 500°C and then characterized.

Characterization of Ceramic Powders Obtained by Controlled Precipitation Method

The ceramic powders synthesized in this work, namely SnO_2 with and without Co, were characterized using various techniques. The functional groups present in the samples, and their evolution, were determined by Fourier transform infrared (FTIR) spectroscopy using a Thermo Nicolet IR 200 spectrometer with the KBr method.

Author's personal copy

Table I. Composition of CoO–SnO_2 systems with different doping percentages obtained by controlled precipitation method

	SnO_2		CoO[a]	
Nomenclature	**wt.%**	**M%**	**wt.%**	**M%**
SnOCoO (0.5%)	99.5	99	0.5	1
SnOCoO (1%)	99	99.8	1	1.99
SnOCoO (2%)	98	96.96	2	3.94

[a]As Co(II) was used in the precursor and the system was not heated to temperatures between 680°C and 700°C, formation of CoO rather than Co_3O_4 is expected.

In this work, thermal analysis was used to determine the temperatures corresponding to the change of the major phase, decomposition of the organic phase, and crystallization. This study was conducted using a Shimadzu DTA-50 differential thermal analyzer in dry air atmosphere at heating rate of 5°C/min with Al_2O_3 as reference.

X-ray diffraction (XRD) analysis was used to study the evolution of the crystalline phases of the suspensions obtained at different stages of the synthesis process and taking into account the different chemical and thermal treatments applied. This study was carried out with a Bruker D8 Advance diffractometer using Cu K_α radiation (λ = 1.54 Å) in the 2θ range from 20° to 100° at 0.02°/min.

The size, morphology, and degree of agglomeration of the synthesized powders were determined by scanning electron microscopy (SEM) using JEOL equipment.

Formation of Ceramic Pieces Using the Colloidal (Slip-Casting) Method

Pieces of SnO_2 ceramic with and without Co were formed by the slip-casting method using stable aqueous suspensions of ceramic powders synthesized by controlled precipitation. To obtain these stable suspensions, the rheological behavior of the mixtures containing the SnO_2 and SnO_2–CoO powders synthesized using water as solvent were studied by adding ammonium polyacrylate (APA) as deflocculant and tetraethylorthosilicate (TEOS) as binder, as indicated in the literature for industrial manufacture of SnO_2 gas sensors.[7]

In previous laboratory-scale work, the viscosity of aqueous suspensions containing different concentrations of solids was measured, and it was found to be possible to obtain stable suspensions with 64% solids. The amounts required for this were 15 g SnO_2 and 8.43 mL distilled water, as calculated using 2.5 g/cm^3 as the theoretical density value for the slip. Of this suspension, 30 mL was used to determine the amount of APA needed to obtain a stable suspension with suitable fluidity (lowest viscosity of the suspension + APA mixture, without flocculation). To do this, APA was added slowly to the suspension containing SnO_2 powder (with or without Co), and the variation in the viscosity of the mixture was recorded using an AG 2000 rheometer. The system pH was also measured.

Having determined the appropriate percentage of deflocculant to use, taking into consideration the optimum values of viscosity, a sufficient quantity of stable suspension was prepared to be able to form pieces with volume of approximately 50 mm^3. The stable slips formed were then subjected to a dispersion process for 6 h using a digital stirrer (IKA model RW-20DS1) to favor the action of the deflocculant and the removal of bubbles from the slurry that could cause structural defects in the cast body. On completion of the dispersion process, the slip was poured into a mold formed by taking 75 g of water per 100 g of calcium sulfate (consistency 75), according to the requirements set out in international standards. The slip was poured into the mold, and once the part acquired a suitable wall size, it was demolded to obtain green material.

For the suspension of SnO_2 and water with tetraethylorthosilicate (TEOS) binder, 1.5 mL TEOS was initially added to the water and then the appropriate amount of APA was determined in order to stabilize it, previously adding 15 g of solids (SnO_2 with and without Co); the APA percentage required to stabilize this suspension was determined using the methodology outlined above.

Dry green pieces were sintered to enhance their densification and obtain the different microstructures required to study the electrical response in the presence of air or CO. Sintering of the samples was carried out in a Carbolite furnace (model RHF 1600) using heat treatments at temperatures of 1000°C, 1100°C, 1150°C, 1200°C, 1250°C, and 1300°C for 2 h.

To compare the microstructure and behavior of the pieces formed by slip casting with the screen-printed thick films normally used in these tests, the latter were formed using synthesized SnO_2 and SnO_2–CoO powders. A paste was formed from these powders by mixing them with glycerol, which was then spread onto alumina substrates with gold electrodes previously deposited by sputtering. On depositing the film, the samples were dried in an

Author's personal copy

oven at 100°C for 12 h to remove part of the organic material. Cooling of the films was carried out quickly, removing the samples from the flask for cooling to proceed at room temperature.

Determination of Gas Sensing Capacity of Films and SnO_2 Ceramic Pieces (with and Without Co)

The gas sensing capacities of the screen-printed thick films and the ceramic pieces formed by slip casting were determined using the equipment shown schematically in Fig. 2. The gases used in this trial were air and carbon monoxide. The active material, i.e., the semiconductor tin dioxide (SnO_2), was located in the sample holder cell of the drain-type, static flow system (Fig. 2), monitoring the variation of the electrical resistance of the active material against the time of exposure to the gas atmosphere of interest at a certain working temperature in the cell. The electrical conductivity behaviors of the films, as a function of temperature, were analyzed using a multimeter (Agilent 34401A).

This system required a pump to remove the air present in the cell containing the semiconductor for analysis. The pump facilitated evacuation of the gas inside, and once the required vacuum was attained, the gas of interest was introduced into the sealed chamber, ensuring the presence of only this gas in contact with the active material. The cell where the active material was placed was furthermore subjected to a given temperature during the test, above room temperature.

Meanwhile, adapting the equipment of Fig. 2, the electrical behavior of the pieces was analyzed using an HP4284A impedance analyzer. The measurements were carried out in the frequency range from 20 Hz to 1 MHz. Measurements of resistance and capacitance versus frequency were then carried out in a furnace. A Novocontrol BDS 1200 commercial temperature controller was used to heat the samples to different temperatures.

RESULTS AND DISCUSSION

Characterization of Synthesized Powders

Fourier transform infrared spectroscopy (FTIR)

Figure 3 shows the FTIR spectra corresponding to solids of the 0.1 M $SnCl_4$ system: after synthesis in aqueous 0.1 N HNO_3 solution at pH 4.2, when washed four times with 0.05 M solution of diethylamine, and after heat treatment at 500°C for 2 h. Bands are observed in the spectra between 614 cm^{-1} and 643 cm^{-1} and at 556 cm^{-1}, which can be attributed to tin oxide.[34–38] Significantly, the bands at 1390 cm^{-1} and between 1623 cm^{-1} and 1635 cm^{-1} were virtually eliminated or diminished in intensity, respectively, when compared with the spectrum corresponding to the aged solid sample. This result indicates that, on washing using diethylamine, the chlorine and nitrate ions present in the samples were removed and that heat treatment favored strengthening of the Sn–O bonds, indicated by the presence of bands between 495 cm^{-1} and 670 cm^{-1}.

Figure 4 shows the evolution of the functional groups present in the samples of cobalt-doped SnO_2, based on their FTIR spectra, for different doping percentages of 0.5 mol.%, 1 mol.%, and 2 mol.% Co.

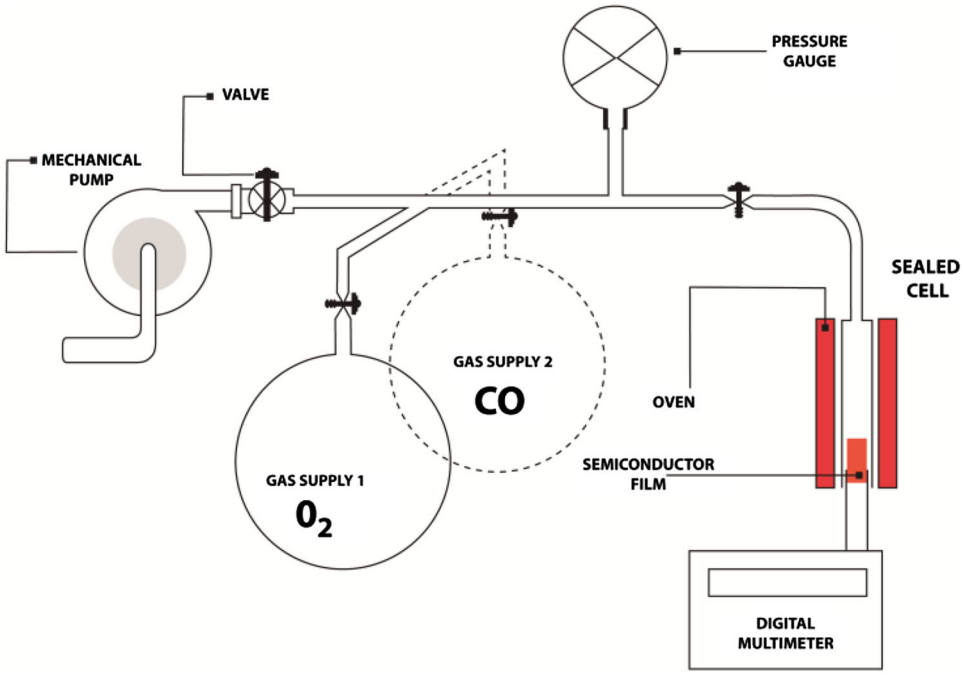

Fig. 2. Schematic of equipment used to determine gas sensing ability of SnO_2 solid.

Author's personal copy

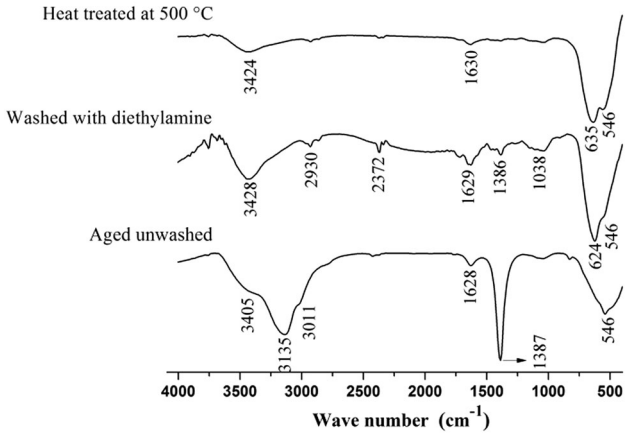

Fig. 3. FTIR spectra corresponding to solid samples of the $SnCl_2$–H_2O–NH_4OH system, synthesized at pH 4.2 and aged for 2 weeks, washed with 0.05 M diethylamine solution, and then heat treated at 500°C.

The solids were washed four times using diethylamine solution and subsequently treated at temperature of 500°C. In these spectra, very well-defined bands can be observed at 611 cm^{-1} to 629 cm^{-1} and 522 cm^{-1} to 560 cm^{-1}, corresponding to tin oxide.[36,37] The results of this study indicate that, on washing using diethylamine, the chlorine and nitrate ions were removed as well as functional groups containing Cl, NH_4, and OH, and with heat treatment, the Sn–O bonds were strengthened.

Thermal Analysis

Figure 5a and b shows the TGA-DTA curves obtained for the synthesized SnO_2 ceramic powders. The TGA curve presents a significant weight loss of about 75% in the range between room temperature and 500°C (Fig. 5a); the initial loss can be associated with outflow of water present in the sample, and the loss between 250°C and 450°C with partial oxidation of organic phase, as well as its dehydroxylation, after which the organic phase is removed completely. In the DTA curve (Fig. 5b), an endothermic peak appears at temperature of ~100°C, corresponding to evolution of water from the solid, while the large exothermic peak at 500°C would indicate oxidation of organic phase and complete crystallization of cassiterite SnO_2.

Figure 5c and d shows the TGA-DTA curves for the samples doped with 0.5 mol.%, 1 mol.%, and 2 mol.% Co. The powders synthesized with different doping percentages exhibit similar behavior, presenting a continuous weight loss up to 250°C (Fig. 5c); the greatest weight loss, observed from this temperature up to 600°C, is due to dehydroxylation of the system and oxidation of organic groups as crystallization of SnO_2 advances. Finally, the weight of the sample remained more or less constant until 900°C. In the DTA curves (Fig. 5d), an endothermic peak appears at 100°C, which can be associated with release of water from the system. In addition, the broad peak at 380°C should indicate the process of dehydroxylation of the sample and decomposition of organic phase present therein. At ~500°C, an intense exothermic peak is observed, which may be associated with complete oxidation of the organic phase and crystallization of cassiterite.

X-ray Diffraction (XRD) Analysis of Synthesized Powders

Figure 6 shows the diffractograms corresponding to the solids obtained at different pH values, washed four times with diethylamine, and heat treated at 500°C. These diffraction patterns indicate that the major crystalline phase is cassiterite SnO_2, confirming the FTIR spectroscopy results in Fig. 3, where the most important functional group was O–Sn–O (band at 635 cm^{-1}).

In the X-ray diffractograms of the samples doped with 0.5 mol.%, 1 mol.%, and 2 mol.% Co and treated at 500°C (Fig. 7), peaks corresponding to cassiterite-phase tin oxide are observed. These peaks undergo slight shifts because of the solid solution formed with CoO. These shifts can be seen by comparing the (110) diffractogram peaks in Fig. 7d.

Morphology and Particle Size of Synthesized Powders

Figure 8a shows SEM images obtained from samples synthesized by the precipitation method and heat treated at 500°C for 2 h. In these images, many agglomerates of about 1 μm are observed, as well as even smaller (<50 nm) particles. The micrographs reveal an irregular and inhomogeneous nanoparticle morphology. Figure 8b shows a SEM image of the sample doped with 2 mol.% Co synthesized by the precipitation method and heat treated at 500°C for 2 h. A large number of hard agglomerates between 1 μm and 5 μm are observed; their presence can be justified considering that the high reactivity of the primary particles and the presence of Co favored mass diffusion during the calcination process, and thus the formation of strong linkages between them. The SnO_2 powders doped with 0.5 mol.% and 1 mol.% Co showed similar characteristics.

Formation of Ceramic Pieces by Slip Casting

Figure 9 shows the curves indicating the variation of the viscosity of the systems of interest, as well as the pH value, when APA was added to suspensions containing 64% SnO_2 solids (with and without Co) synthesized by controlled precipitation. Figure 9a shows the evolution curve of the viscosity and pH variation for a suspension concentrated in SnO_2 (64% solids), as a function of the amount of APA deflocculant. The minimum value of the viscosity of the suspension, 0.159 N s/m^2 (159 cP) was achieved on adding 0.2 mL deflocculant to 30 mL

Author's personal copy

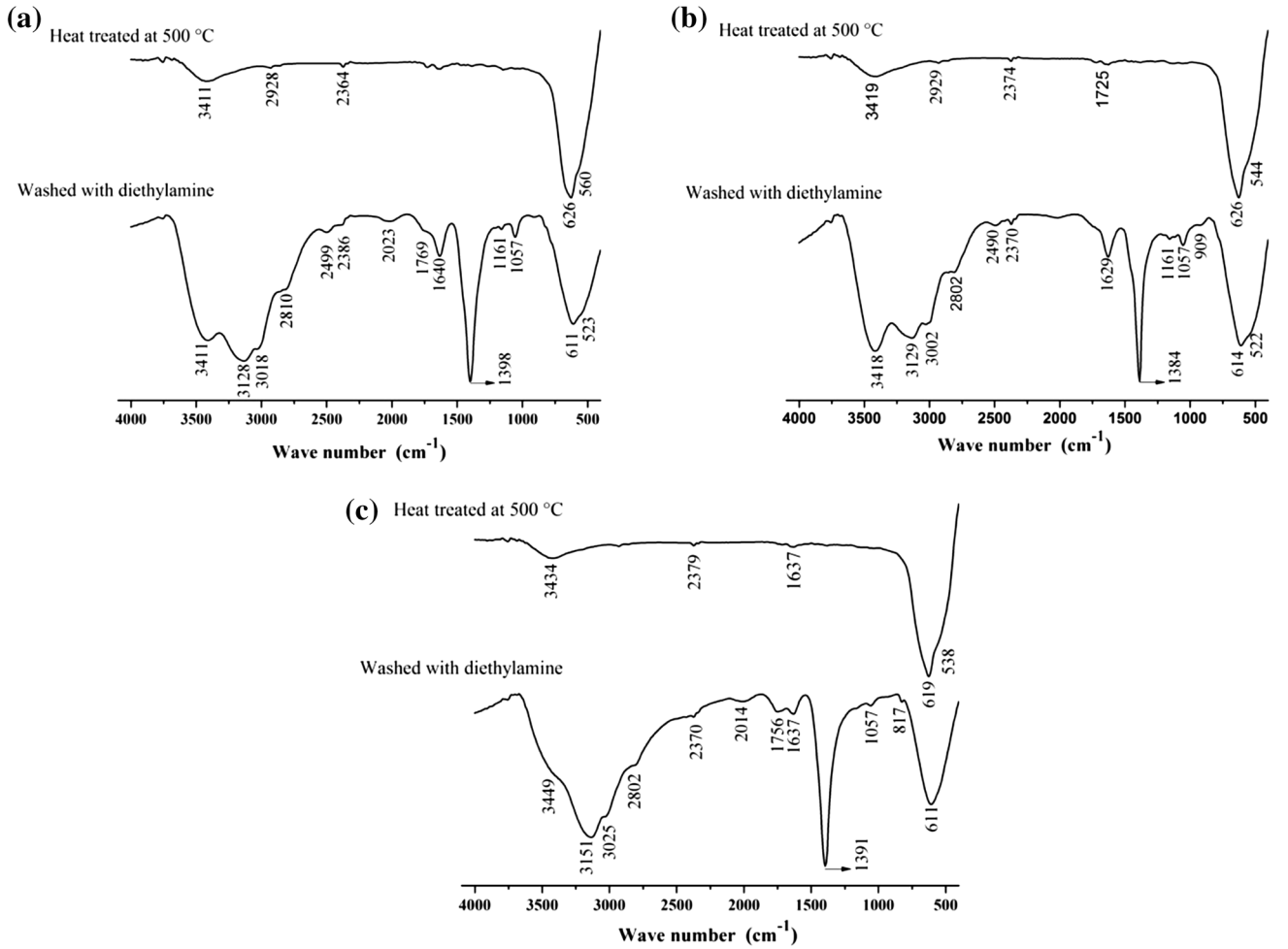

Fig. 4. FTIR spectra corresponding to solid samples of the SnO_2–CoO system aged for 2 weeks, washed with 0.05 M diethylamine solution, then treated at 500°C, containing different mol percentages of Co doping: (a) 0.5%, (b) 1%, and (c) 2%.

suspension, resulting in stabilization of the suspension. This was then used for casting the pieces.

In the case of the suspension of SnO_2 and water with TEOS (concentration 5%) (Fig. 9b), the curve indicates that, with 0.245 mL APA, a stable slip was obtained with viscosity of 0.373 N s/m^2 (373 cP). Examining the variation in pH of the suspensions, on addition of APA (Fig. 9), it was seen that the minimum viscosity values correlated with the maximum pH values. A similar outcome was observed for the suspension of SnO_2 with 2 mol.% Co (Fig. 9c). In this curve, the viscosity was seen to reach a minimum value of 0.415 N s/m^2 (415 cP) on addition of 0.22 mL APA.

The pieces sintered at 1250°C for 2 h were characterized by SEM to determine the morphology and size of the grains, as well as the porosity present. To do this, the sintered material was broken and the fractured surface of the samples observed. Figure 10 shows the microstructure of the different ceramic pieces of interest, formed by the casting method, using SnO_2 powders synthesized by controlled precipitation. The pieces obtained from suspensions stabilized by APA and containing TEOS (Fig. 10a) showed high porosity and low homogeneity in their microstructure, indicating inadequate densification of the material. The presence of agglomerates in the initial ceramic powder (Fig. 8) should have promoted both intra- and interagglomerate sintering.

Unlike Fig. 10a, the micrograph of the sample doped with 2 mol.% cobalt (Fig. 10b) showed a more homogeneous microstructure, with clear presence of pores and grain size of about 1 μm. From Fig. 10, it can be seen that the pieces formed by the slip-casting method showed different kinds of intergranular contacts (Fig. 1), with a more uniform structure for the samples doped with Co (Fig. 10b). Given the late-stage neck growth at high temperatures (see Fig. 3.2 of Ref. 32) in the sintering process (T = 1250°C in this work), a large number of grains were connected via necks, coming closer to each other and thus reducing the distance between their centers, due to the action of mass diffusion mechanisms that promote densification (principally diffusion through grain boundary and diffusion through

Author's personal copy

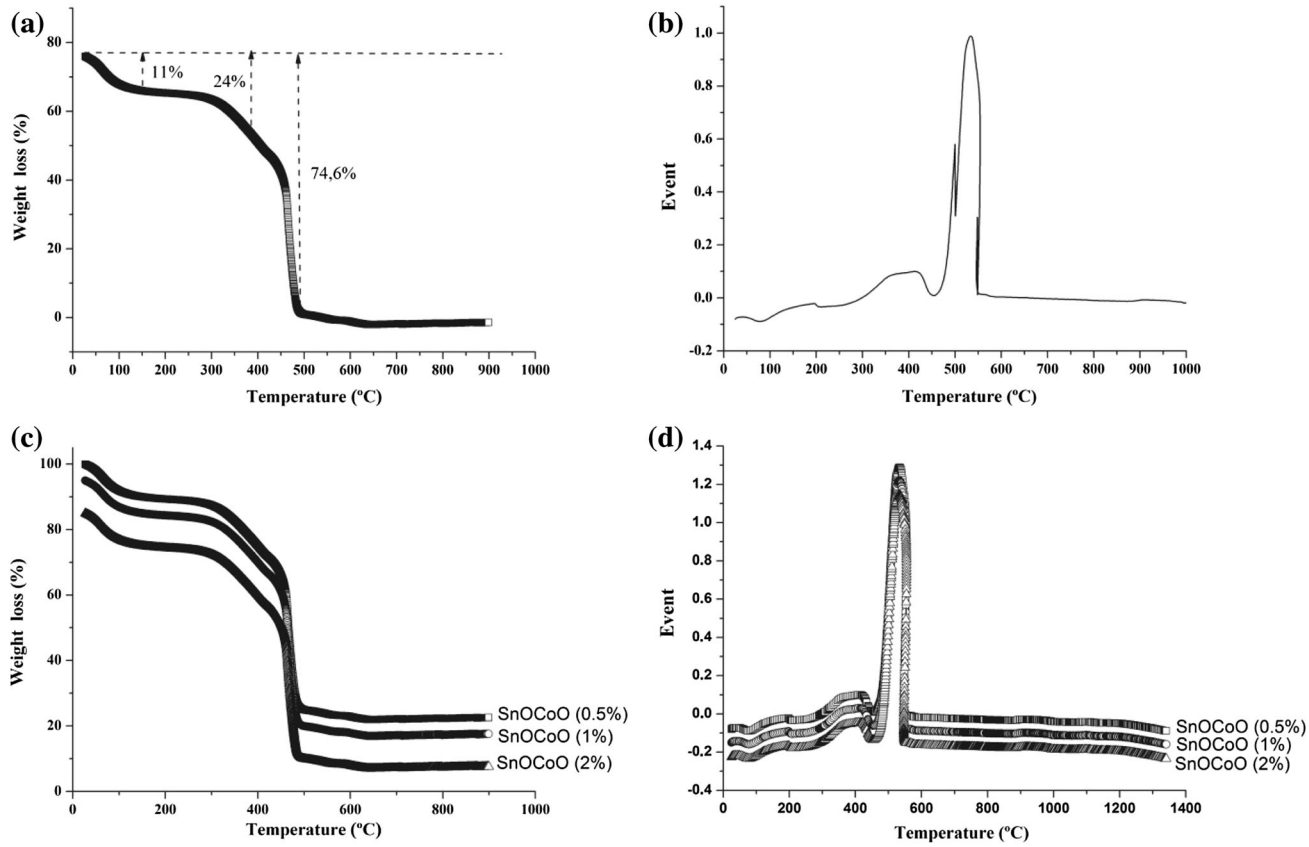

Fig. 5. TGA and DTA curves corresponding to SnO_2 ceramic powders obtained by controlled precipitation method (a, b) without Co and (c, d) doped with different concentrations of Co.

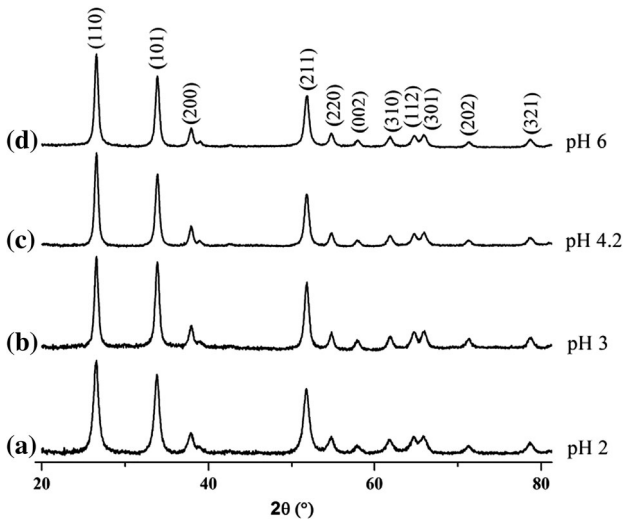

Fig. 6. X-ray diffractograms corresponding to solid samples of the $SnCl_2$–H_2O–NH_4OH system washed four times using 0.5 M diethylamine solution and heat treated at 500°C, obtained at pH values of (a) 2.0, (b) 3.0, (c) 4.2, and (d) 6.0.

bulk). This causes the grain boundary to begin to disappear, leading to grains in a state of coalescence and an apparent continuity of mass in this zone (see Fig. 3.2 of Ref. 32), a process that favors the formation of open necks. The existence of closed necks in the microstructure cannot be ruled out due to the sintering process not achieving complete densification of the part, but coarsening events are also evident (Fig. 10a and b), encouraged by transport mechanisms such as surface diffusion or evaporation–condensation.[32] Therefore, considering the potential use of these porous pieces as gas sensors and given the microstructure of the SnO_2 pieces formed (Fig. 10a and b), it is possible that there are three distinct contributions to the electrical conduction mechanism in this porous material: surface/bulk (for large necks), grain boundary (for large grains not sintered together), and flat bands (for small grains and small necks), leading to paths with low electrical resistance through the bulk of the crystallites and open necks, alternating with zones of high resistance at some contact points.[9,10,14,39]

Figure 10c and d shows SEM images of the thick films formed with ceramic powders of the SnO_2 and SnOCoO (2%) systems (SnO_2 powder doped with 2 mol.% Co); the latter sample was chosen for this study, taking into account the microstructural development and the homogeneity of its porosity. In this figure, the formation of particle aggregates can be seen, representing a condition that must appreciably influence the electrical behavior of the thick films.

Author's personal copy

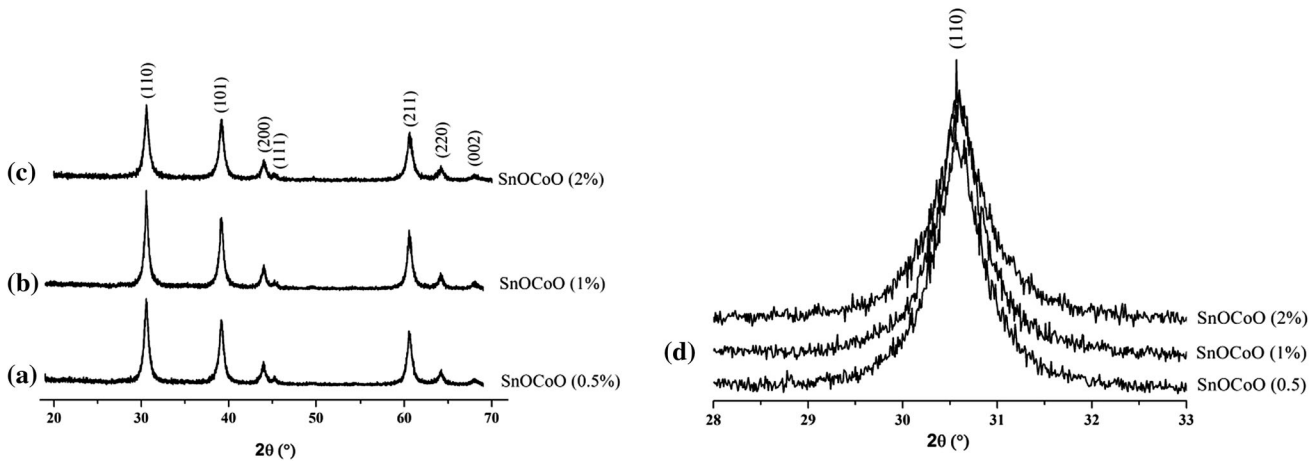

Fig. 7. X-ray diffractograms corresponding to solid samples of the SnO_2–CoO system washed using 0.05 M diethylamine solution and heat treated at 500°C, obtained for Co doping percentages in mol of (a) 0.5, (b) 1, (c) 2%, and (d) (110) peak for each sample.

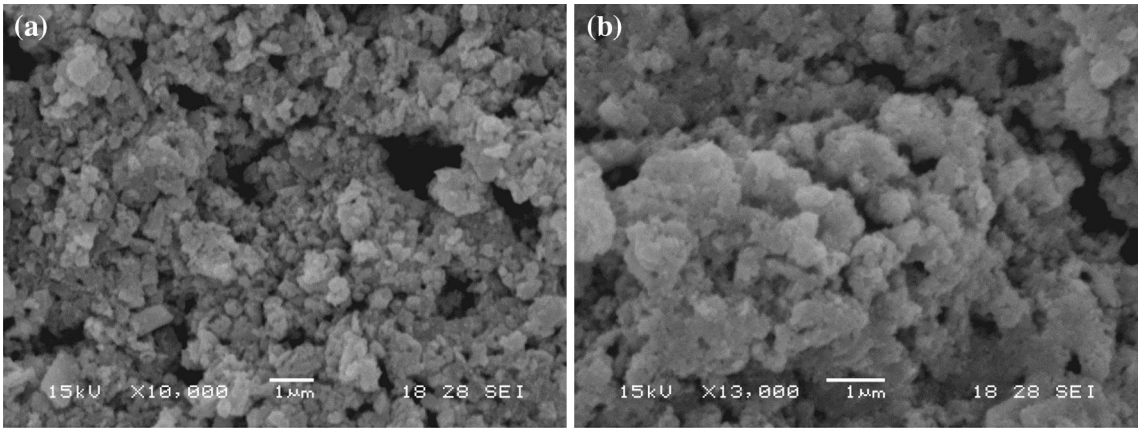

Fig. 8. SEM images corresponding to SnO_2 system ceramic powders synthesized by controlled precipitation method and heat treated at 500°C for 2 h: (a) without cobalt and (b) doped with 2 mol.% Co.

The presence of cobalt was important for the densification of the pieces formed using the powders synthesized in this work, as shown in Fig. 10b and d. Cobalt promoted activation of the densification mechanism, as can be appreciated by considering the formation of oxygen vacancies through the following reaction:

$$CoO \xrightarrow{SnO_2} Co_{\ddot{S}n} + V_{\ddot{O}} + O_O^x \qquad (1)$$

where Co^{2+} would replace Sn^{4+}. These oxygen vacancies would contribute to "mass transport," specifically of oxygen, and to its rapid spread across the grain boundaries; on adding 2% cobalt by weight to SnO_2, it becomes more densified, reaching ~94% of theoretical density. Furthermore, the presence of $V_{\ddot{O}}$ in the material structure is favorable for gas sensing, facilitating oxygen diffusion.[40,41]

Gas Sensing Capacity of SnO_2 Ceramic Pieces Formed by Slip Casting

Variation of Electrical Resistance of Active Material in Presence of Air

To determine the most suitable temperature for electrical characterization of the pieces formed by slip casting (Fig. 10a and b) from the SnO_2 powders (with and without Co) synthesized in this work, the equipment shown in Fig. 2 was used, placing the thick films (Fig. 10c and d) in the presence of air. The curves in Fig. 11 show the electrical resistance of the thick films versus exposure time to 30 mmHg air at different working temperatures, indicating that the maximum resistance achieved decreased with increasing working temperature. Initially, the curves showed an increase in resistance, after a

Author's personal copy

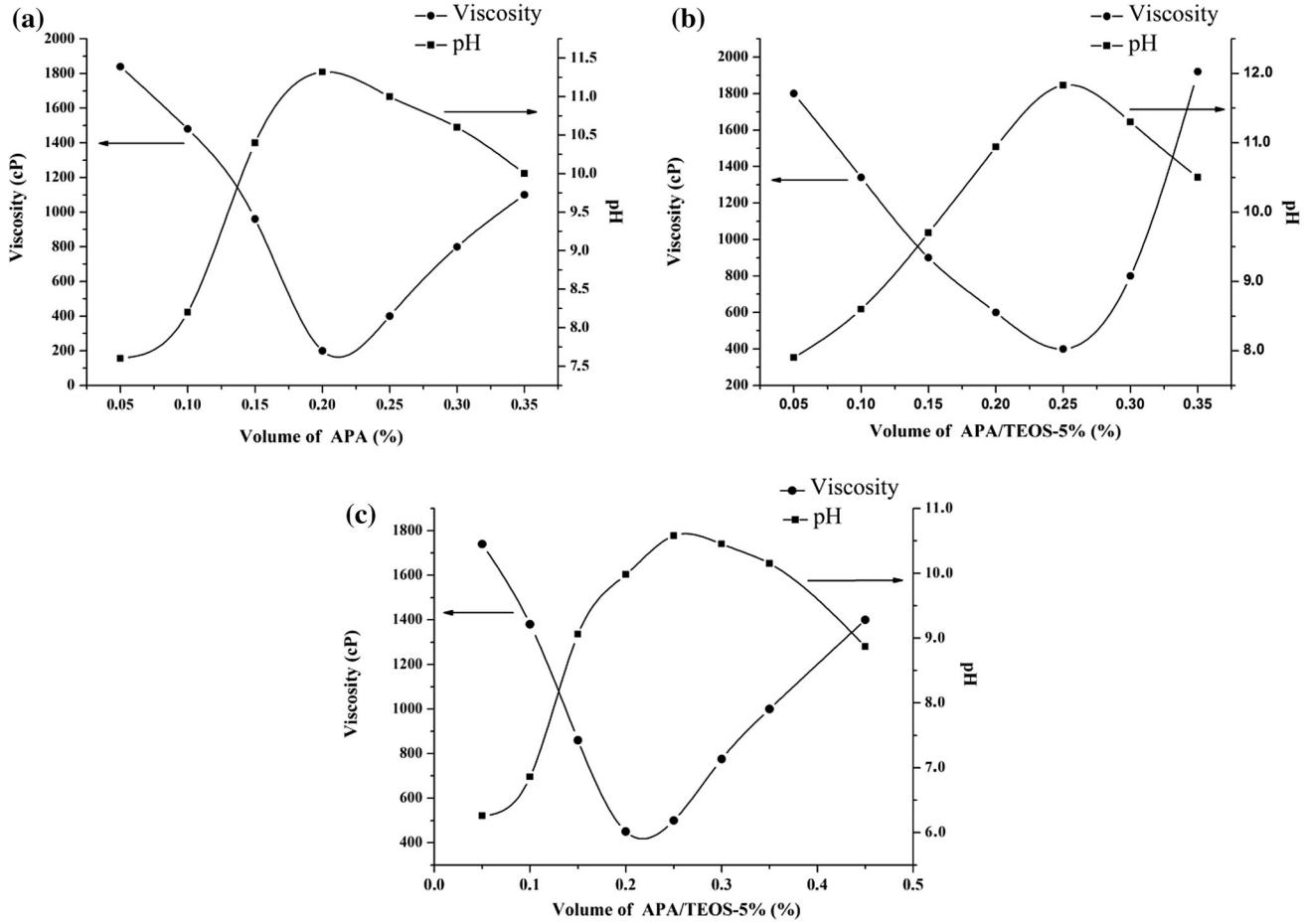

Fig. 9. Variation of viscosity and pH of suspensions (30 mL, 64% solids) formed using SnO_2 synthesized by controlled precipitation and distilled water on adding (a) APA, (b) APA and TEOS (5%), and (c) SnO_2–2 mol.% Co with APA–TEOS (5%).

time reaching a saturation condition (maximum resistance), the resistance value of which decreased as the working temperature was increased; the resistance of the samples was not as well differentiated at the working temperatures of 280°C and 350°C. In addition, for samples tested at the highest temperatures, the resistance in the saturation zone decreased with time.

Based on the curves in Fig. 11, 280°C was chosen as the working temperature for electrical characterization of the ceramic pieces, since there was a significant increase in the resistance of the part, with an approximately constant value in the saturation zone.

The curves in Fig. 12 show the electrical behavior of samples formed by screen printing and slip casting using nondoped SnO_2 powder (Fig. 12a) and powder doped with 2% Co (Fig. 12b) as a function of exposure time to an oxidizing atmosphere at 280°C. Figure 12 shows that the resistance of the samples depends on the method used to form the part tested, as well as on the presence of cobalt. The variation of the resistance is slightly greater with the presence of air, for the pieces obtained by slip casting.

Electrical Behavior of Slip-Cast Ceramic Pieces in Presence of a Gas

To determine the effect of the presence of a gas on the electrical behavior of the pieces obtained by slip casting using SnO_2 powder doped with 2 mol.% Co—which were those showing the most homogeneous pore structure (Fig. 10b)—the technique of complex impedance spectroscopy was employed. Electrical measurements were taken on sintered samples exposed to air or carbon monoxide atmosphere at 280°C. The measures of interest (principally the resistance and capacitance in parallel) were determined using an HP 4192 impedance analyzer in the frequency range from 5 Hz to 1 MHz, using the appropriate computer support for data acquisition and processing.

Figure 13 illustrates the change in the resistance R_p as a function of frequency for the SnO_2 film with 2 mol.% Co exposed to air atmosphere (30 mmHg) at 280°C when applying different bias voltages. As indicated by the curves in Fig. 13, on introducing air into the chamber where the sample was located, a change was observed in the electrical resistance, specifically a sharp decrease at high frequencies.

Author's personal copy

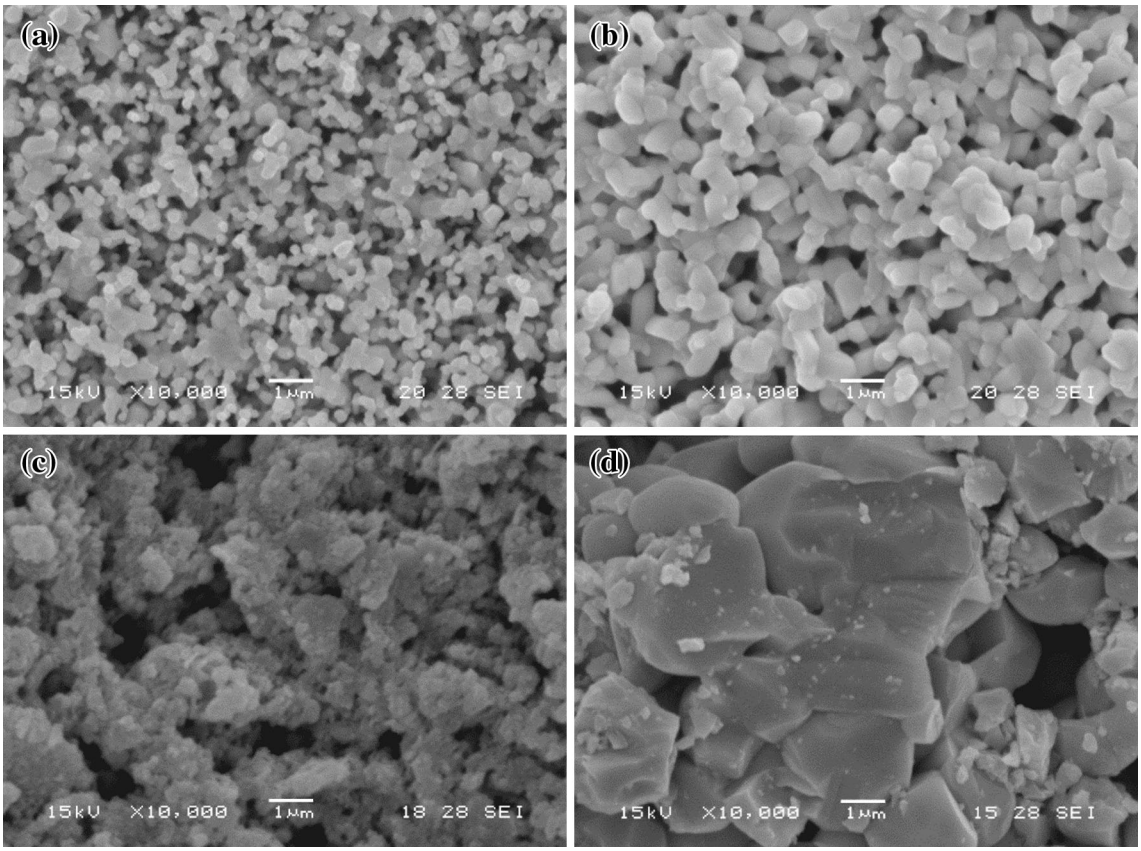

Fig. 10. SEM micrographs corresponding to pieces sintered at 1250°C formed with SnO_2 suspensions synthesized by controlled precipitation, on addition of APA and TEOS (5%) to SnO_2 without Co (a) and doped with Co (2 mol.%) (b); SEM images of film made by the screen-printing method, using ceramic powders from the SnO_2 systems without Co (c) and SnOCoO (2%) (d), synthesized by the controlled precipitation method.

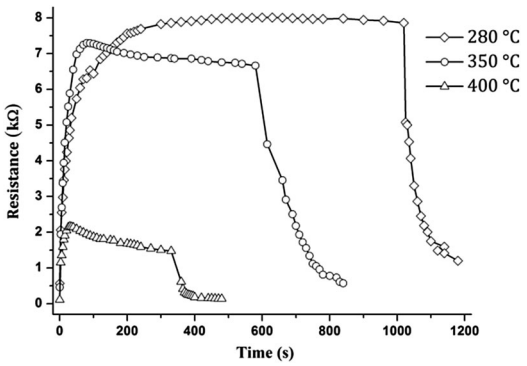

Fig. 11. Variation of the resistance of thick films formed with SnO_2 system powders synthesized in this work with time at temperatures of 280°C, 350°C, and 400°C in presence of air (30 mmHg).

Figure 14 shows the response of the capacitance C_p of SnO_2 films doped with 2 mol.% Co as a function of frequency at 280°C, for different bias voltage values. The curves show that the response of the capacitance remains almost constant at high frequencies. However, at frequencies below ~1000 Hz, the behavior of the curve at bias voltage of 0 V (Fig. 14a) presented a different behavior from that observed at the bias voltages of 10 V (Fig. 14b), 20 V (Fig. 14c), and 30 V (Fig. 14d), i.e., the capacitance increased as the frequency decreased.

In discussing the above results, it should be noted that SnO_2 is an *n*-type ceramic semiconductor and that a combination of two types of intergranular contact predominate in its structure (compare Fig. 1 with Fig. 10b): a predominance of open necks or bridges and those that can be represented by Schottky barriers, representing a combination of contributions to the electrical conduction from both double Schottky barrier type and surface traps and defects in the bulk (shallow and deep). This should be borne in mind when accounting for the electrical behavior of the ceramic pieces.

The admittance results, i.e., R_p and C_p as a function of frequency (Figs. 13 and 14), can be justified by considering the effects of relaxation, due to both the finite response time of the load on the interface, such as the states of bulk defects, as well as the independence of the time constant of deep traps from the bias voltage applied to the device.[42]

An important aspect to consider in understanding the electrical behavior of SnO_2 is that the charge balance in the intergranular zone involves electrons trapped both in the states of the interface (N_i) and in

Author's personal copy

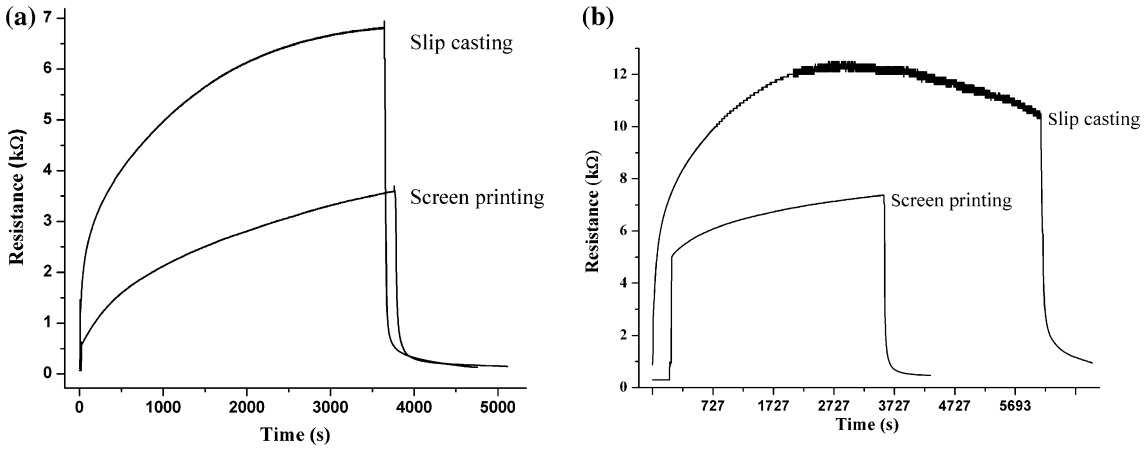

Fig. 12. Curves of electrical resistance at 280°C versus exposure time to an oxygen atmosphere for films formed by screen printing and slip casting using SnO_2 powders without doping (a) and doped with 2 mol.% Co (b).

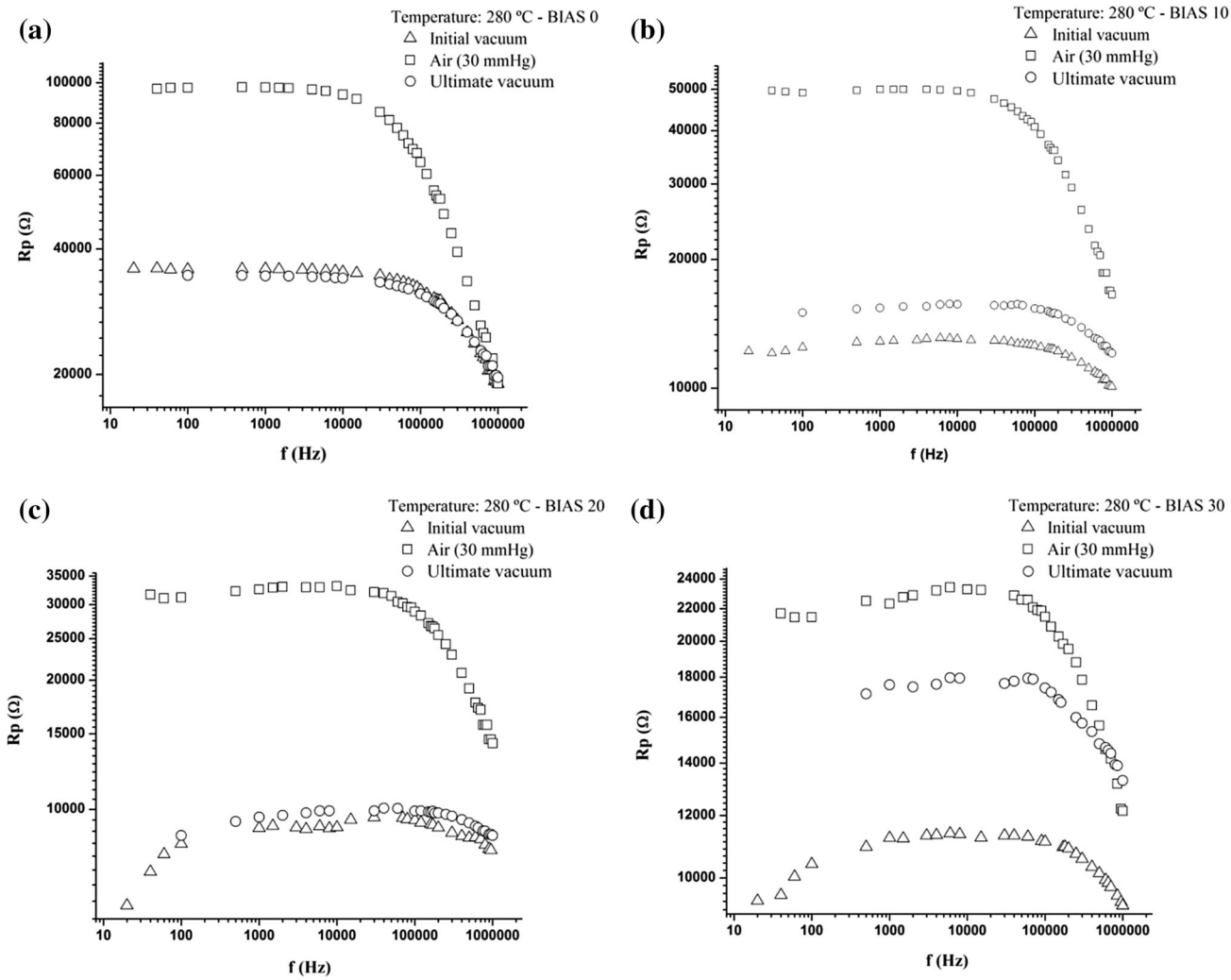

Fig. 13. Variation in resistance as a function of frequency of SnO_2 films with 2 mol.% Co exposed to air atmosphere (30 mmHg) when applying different bias voltages of (a) 0 V, (b) 10 V, (c) 20 V, and (d) 30 V at 280°C.

Author's personal copy

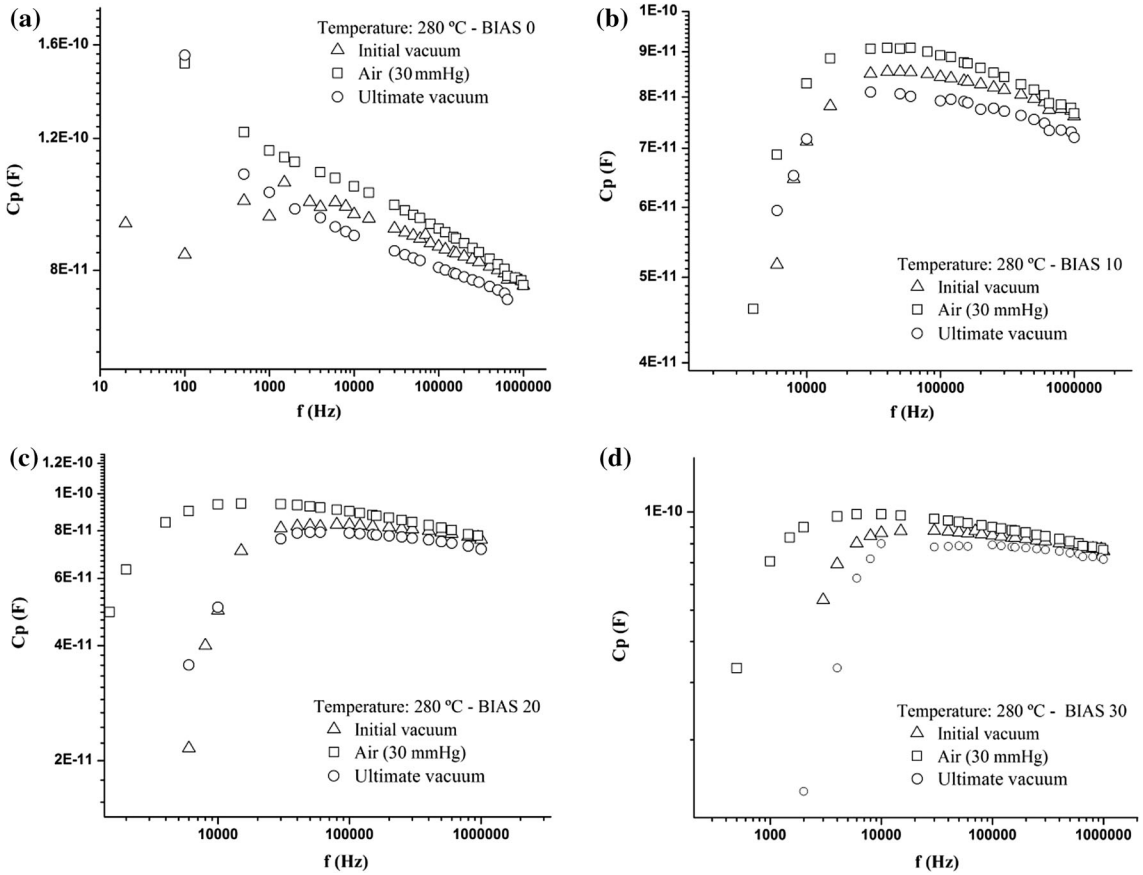

Fig. 14. Variation of capacitance of film of SnO_2 with 2% Co as a function of frequency when exposed to air atmosphere (30 mmHg) for different bias voltages of (a) 0 V, (b) 10 V, (c) 20 V, and (d) 30 V at 280°C.

the shallow (N_D) and deep (N_v) defects. This means that the key parameters that determine, for example, the value of the potential barrier $\Delta\phi_B$, are: (i) the doping level N_D, N_v of the grains of SnO_2, (ii) the total interfacial charge Q_i, and (iii) the current distribution of the density of states in the interface, $N_i(E)$.[43]

As previously stated, to understand the electrical behavior of the SnO_2 doped with cobalt as shown by the parallel equivalent curves of resistance and capacitance as a function of frequency (admittance measures[44]) with varying bias voltage at 280°C (Figs. 13 and 14), one should consider the effect of the two types of traps on the carriers, principally electrons, that produce electrical conduction: (1) the traps located at the interface and (2) those localized in the semiconductor bulk (shallow defects and deep traps in the grains of SnO_2 and point defects $V_{\ddot{O}}$ and $V_{\dot{O}}$ for the most part).

Specifically, for pure SnO_2, deep defects are not expected, and only the shallow type will be present.[45,46] However, incorporation of cobalt should induce states in the gap, near in half thereof,[47] as well as states associated with $V_{\ddot{O}}$ that are generated during the process of compensation for the charge imbalance brought about by substitution of Sn^{4+} by Co^{2+}. Thus, deep defects (traps) will originate in the material.

Furthermore, to understand the effect of the bias voltage on the electrical behavior of the pieces, taking into account the effect of frequency (f) in the alternating-current (AC) measures of the electrical behavior of the intergranular zone as observed in other systems,[48] it is necessary to consider the characteristic frequencies of capture (C_n) and emission (e_n) of carriers in the limit of probability of occupation of the interface states. The results obtained indicate that three different frequency ranges can be distinguished qualitatively, with the following characteristics:[48]

(a) A range of high frequencies, $f \gg$ characteristic frequencies of (e_n, C_n), where the charge of the interface Q_i remains constant during a modulation cycle of the signal.
(b) A range of low frequencies, $f \ll$ characteristic frequencies of (e_n, C_n), where Q_i varies in phase with the applied signal.
(c) An intermediate range, where f is approximately equal to the characteristic frequencies of (e_n, C_n), such that Q_i exhibits a time dependence on the frequency f but is not in phase with the signal modulation.

Author's personal copy

Considering the statement above, and observing the curves of R_p and C_p (Figs. 13 and 14), the effect of the states of the grain boundary (traps for the electrons) is evident in the curves of capacitance C_p (Fig. 14) as would be expected:[42,43,49] at high frequencies, the capacitance remains practically constant, because the charge Q_i does not change, while at low and intermediate frequencies there should be large "resonances" or dependencies on Q_i with time that should result in changes in C_p. On the other hand, there should be changes in the transition from one type of behavior to another, as shown in the C_p curves, on varying the bias voltage V, due to the dependence of the degree of occupation of the interface states on this voltage.

Another important change in the values of R_p and C_p (Figs. 13 and 14) is seen on changing the atmosphere surrounding the SnO_2 part doped with cobalt from vacuum to air, as most readily observed in the curves of R_p rather than C_p. Previous studies carried out with n-type semiconductors, principally ZnO,[47] suggested that presence of oxygen at the surface and intergranular zones of the material primarily affects the barrier height, such that on its removal from these zones, the height is reduced, facilitating the passage of current carriers (increasing, for example, leakage currents in the case of the ZnO varistor[47]), a behavior that accounts for the reduction in the resistance observed in the R_p curves in Fig. 13 when testing the sample in vacuum.

Another important parameter is the bias voltage. On increasing its value, the equivalent resistance in parallel R_p is reduced, as shown in Fig. 13. Furthermore, the conductance is much more sensitive to the presence of deep traps in the bulk,[49] which would explain the behavior shown by the R_p curves at high frequencies, where the mechanism of traps would be the most important[50] (Fig. 13).

Looking specifically at the C_p curves (Fig. 14), the presence of oxygen in the atmosphere surrounding the sample only very slightly affects the capacitance values of the part at high frequency values. The main change occurs at low frequencies, affecting mostly the frequency value at which the transition from one type of behavior to another occurs. Changes in the bias voltage bring about a very obvious effect on the behavior of the parallel capacitance of the part: at low and intermediate frequencies a change in behavior of the values of C_p occurs when moving from zero to finite bias voltage (Fig. 14). For zero bias voltage, usually the shallow donors provide the

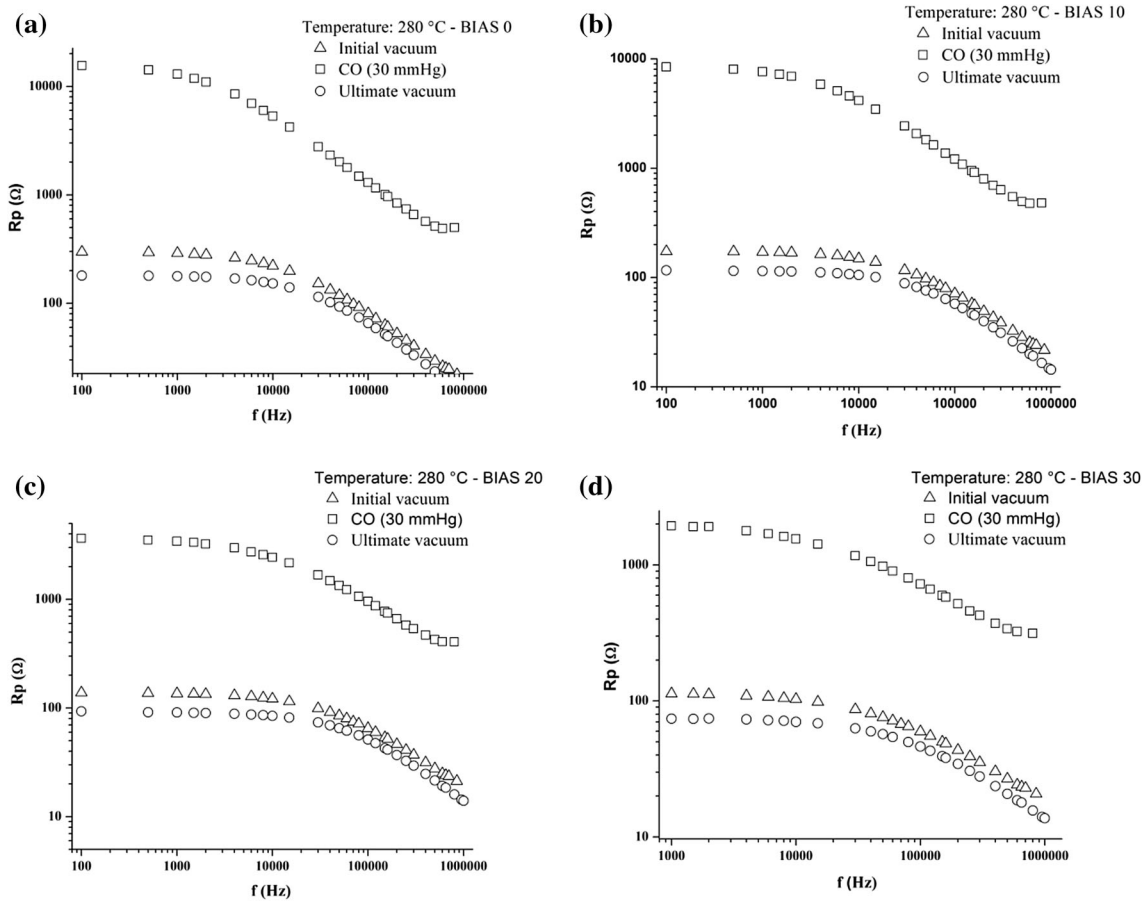

Fig. 15. Variation of resistance as a function of frequency for SnO_2 ceramic pieces doped with 2 mol.% Co when exposed to atmosphere of CO (30 mmHg) for different bias voltages of (a) 0 V, (b) 10 V, (c) 20 V, and (d) 30 V at 280°C.

Author's personal copy

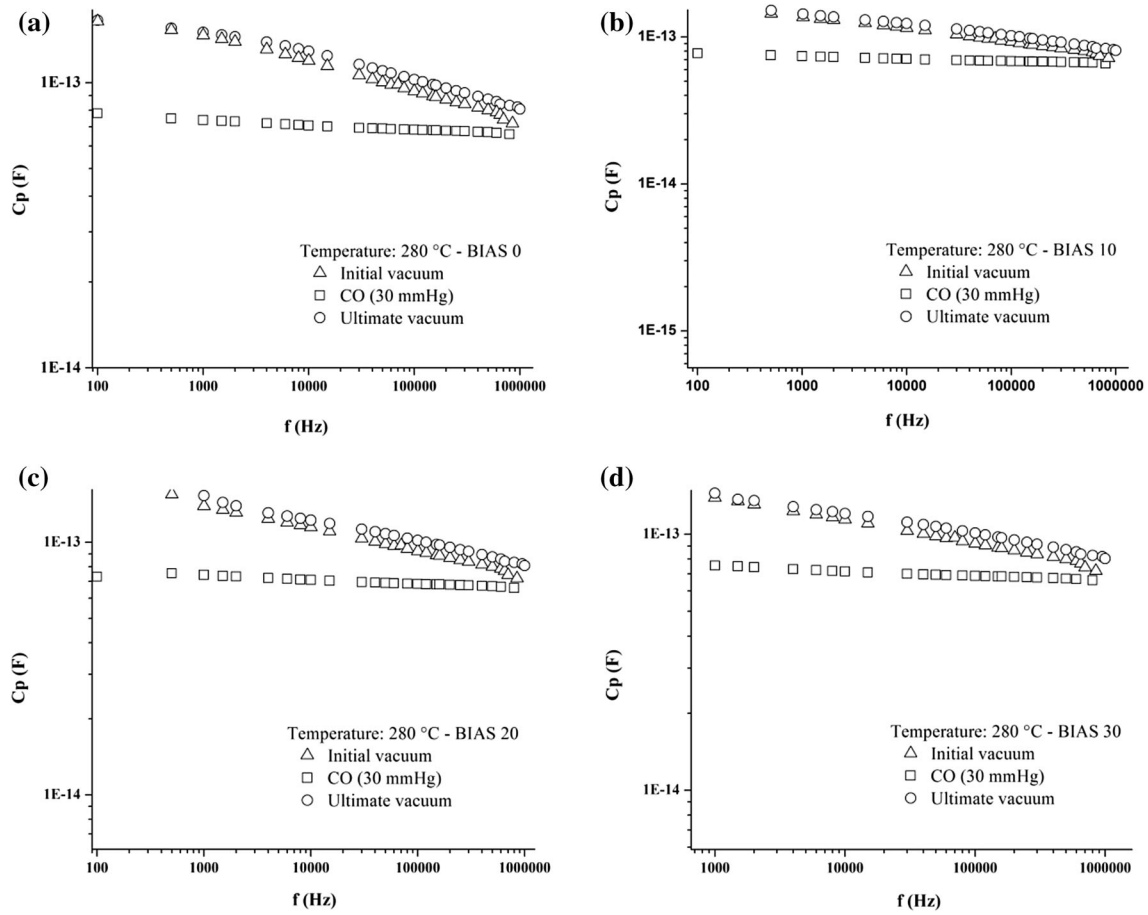

Fig. 16. Variation of capacitance as a function of frequency of porous SnO_2 pieces doped with 2 mol.% Co exposed to atmosphere of CO (30 mmHg) for different bias voltages of (a) 0 V, (b) 10 V, (c) 20 V, and (d) 30 V at 280°C.

greatest portion of screening charge, so that the capacitance would be essentially constant over the entire frequency range,[49] except at low frequencies (in the present case for $f < 100$ Hz) where scattering phenomena are seen (low-frequency dispersion, LFD), due to the finite and reversible accumulation of charge in the bulk or at the interface.[44,49,51]

Although in this analysis the effects of traps located in the grain boundary and within the space-charge region on the electrical activity of SnO_2 have been considered separately, in actual systems these act simultaneously. It is possible, therefore, that the emission of charge carriers from the interface states coincides with the capture of carriers by the traps, or that the emission from the latter coincides with the capture of carriers in the interface.[48] These processes of capture and emission would therefore produce opposing changes in the capacitance of the grain boundary, with very different kinetics. One effect that has been extensively studied, using the model applied above, is the anomalous behavior shown by the capacitance of the semiconductor at low frequencies: at these frequency values, the capacitance reduces in value, reaching negative values (inductive behavior), on increasing the value of the bias voltage V applied to the semiconductor,[42,43,49–51] as observed in Fig. 14.

Figure 15 shows the variation of the resistance R_p as a function of frequency for porous SnO_2 pieces doped with 2 mol.% Co formed by the colloidal method, when the sample is subjected to a vacuum and subsequently exposed to an atmosphere of 30 mmHg CO at 280°C. The electrical resistance decreased with frequency such that, for certain values of frequency, these changes were far more evident, and finally, around 1 MHz, the resistance remained at an almost constant value. The behavior of the curves in Fig. 15 in the presence of CO is different from those in Fig. 13 in air, with higher resistance (lower conductivity) values found in the latter, highlighting the fact that the electrical response of the porous active material strongly depends on the nature of the surrounding gas.

In Fig. 16, the response of the capacitance C_p of the SnO_2 pieces doped with 2% Co is illustrated as a function of frequency at 280°C for different applied bias voltages. The curves show that the capacitance value of the porous active sample remains practically constant in the frequency range used for the test. As for the behavior of the R_p values of the

Author's personal copy

samples tested in air (Fig. 13) and CO (Fig. 15), the capacitance of the porous active material also depended heavily on the nature of the sensed gas, i.e., oxygen (Fig. 14) or CO (Fig. 16), with greater capacitance values when O_2 was used as the surrounding atmosphere during the test.

To account for the results shown in Figs. 15 and 16, it should be noted that, when conducting the test using CO, a substantial quantity of surface oxygen vacancies, $V_{\ddot{O}}$, are generated in the sample as a result of the interaction of CO with the SnO_2 surface, and surface tin Sn^{4+} may be reduced, resulting in Sn^{2+} through the reaction

$$Sn_{Sn}^{x} + 2e' \rightarrow Sn_{Sn}'' \quad (2)$$

Surface vacancies, at the working temperature, would disseminate into the SnO_2 interior, where they would act as donor vacancies. On increasing the concentration of $V_{\ddot{O}}$, this condition could affect the value of the concentration of deep traps, N_v, increasing their quantity and thereby reducing the barrier height ϕ_B; this would result in an increase in the conductivity of the active material (reducing its resistance). Furthermore, the reduction of Sn^{4+} would cause a decrease in the amount of electrons in the conduction band, according to Eq. 2, leading to a decrease in conductivity and therefore an increase in the electrical resistance of the sensor.

Although these two mechanisms would act simultaneously during the course of the test, introduction of CO at the working temperature should favor the reduction of Sn^{4+} to Sn^{2+} through Eq. 2 more than the generation of $V_{\ddot{O}}$, so electrons would have been taken from the conduction band during the reduction of the tin ion (Eq. 2), which would cause the electrical resistance of the material to increase, as shown in Fig. 15. As mentioned previously, the deep traps have a greater effect on R_p at high frequencies, so that, observing the curves in Fig. 15, these affect the samples tested in a vacuum more than when exposed to CO. This behavior becomes more noticeable on increasing the value of the bias voltage.

Observing the behavior of the C_p curves (Fig. 16), it can be concluded that they do not show great variations when the porous active material is in the presence of CO because the charge of the interface Q_i remains virtually constant. Furthermore, the small variation shown by the cobalt-doped SnO_2 in vacuum is a progressive decrease, virtually linear in the frequency f; i.e., the charge of the interface Q_i would vary with frequency, causing a slight change in the capacitance.

CONCLUSIONS

Porous pieces of SnO_2 ceramic with and without Co were obtained in a reproducible and controlled way using the slip-casting method. The methodology used to form the pieces, with a suitable sintering program, allowed control over their final microstructure, specifically the porosity, obtaining better results on cobalt addition. The pieces displayed normal behavior in the sintering process, following the stages typical of sintering of porous bodies, with the growth of large rather than small pores being favored, and likewise for grain growth, as well as, in some cases, decreasing distance between the joined grains (densification) albeit not reaching complete densification of the part (development of coarsening events during sintering).

The sample with 2 mol.% cobalt sintered at 1250°C for 2 h was selected for electrical characterization and SEM study, showing a predominance of open necks or bridges (due to the late-stage neck growth that would occur at this treatment temperature) and intergranular contacts that can be represented by Schottky-type barriers, with a very small number of closed necks being evident. Since these two types of intergranular contact were dominant in the porous structure of this material, the factors determining the electrical behavior and conductivity of the active material would be expected to be the presence of Co in the solid, the fractional coverage of gas species, and the nature of this gas (air or CO). The results of electrical characterization of the selected ceramic part bear this out, indicating that its conductivity would be controlled by the shallow and deep traps in the bulk, brought about in part by the presence of Co, and by the barrier height and width, determined by the charge and the coverage of surface species from the surrounding gas.

Furthermore, because the grains have different shape, size (around 1 μm), and form, and there is a statistical distribution of defects and dopant (cobalt) on the surface of the grains, a wide distribution in barrier height is expected, which would generate a random, inhomogeneous arrangement in the energy profile of the bottom of the conduction band, apparently resulting in a percolation network in the material, generated by the presence of open-neck domains where the movement of charge carriers is relatively easy, and Schottky-type barriers where it is more difficult. Additionally, given the relatively small grain size (about 1 μm), a major contribution to the electrical conduction mechanism in the porous active material would come from flat bands, since the grains might be depleted of conduction electrons and the conductivity would be limited by electron excitation from traps at grain boundary.

Finally, the results of electrical characterization of the sample indicate that the R_p and C_p curves exhibit different behavior, and different values, depending on the nature of the gas (air or CO) and the bias voltage applied. This difference is most evident in the C_p curves, a behavior that is consistent with the nature and characteristics of the microstructure of the porous active material studied.

Author's personal copy

ACKNOWLEDGEMENTS

We are grateful to the VRI of the University of Cauca for funding Project ID 2731 and for providing logistical support. We are especially grateful to Colin McLachlan for suggestions relating to the English text.

REFERENCES

1. W.H. Brattain and J. Bardeen, *Bell Syst. Technol. J.* 32, 1 (1953).
2. G. Heiland, *Z. Phys. A* 138, 459 (1954).
3. M.J. Madou and S.R. Morrison, *Chemical Sensing with Solid State Devices* (Boston: Academic, 1989).
4. E. Comini, G. Faglia, and G. Sberveglieri, eds., *Solid State Gas Sensing* (New York: Springer Science, 2009).
5. R. Jeaniso and O.K. Tan, eds., *Semiconductor Gas Sensors* (Cambridge: Woodhead, 2013).
6. G. Eranna, *Metal Oxide Nanostructures as Gas Sensing Devices* (Boca Raton: Taylor & Francis, CRC, 2012).
7. K. Ihokura and J. Watson, *The Stannic Oxide Gas Sensor* (New York: CRC Press, 1994).
8. W. Hagen, R.E. Lambrich, and J. Lagois, *Adv. Solid State Phys.* 23, 259 (1983).
9. J.F. McAleer, P.T. Mosley, J.O.W. Norris, and D.E. Williams, *J. Chem. Soc. Faraday Trans.* 1, 1323 (1987).
10. LYu Kupriyanov, eds., *Semiconductor Sensor in Physicochemical Studies*, vol. 4 (Amsterdam: Elsevier Science, 2002).
11. N. Yamazoe, *Sensors Actuators B Chem.* 5, 7 (1991).
12. W. Göpel and K.D. Schierbaum, *Sensors Actuators B Chem.* 26, 1 (1995).
13. C.C. Wang, S.A. Akbar, and M.J. Madou, *J. Electroceram.* 2, 273 (1998).
14. N. Barsan and U. Weimar, *J. Electroceram.* 7, 143 (2001).
15. N.M. Beekmans, *J. Chem. Soc. Faraday Trans.* 1, 31 (1978).
16. J.O. Cope and I.D. Campbell, *J. Chem. Soc. Faraday Trans.* 1, 1 (1973).
17. S. Baidyaroy and P. Mark, *Surf. Sci.* 30, 53 (1972).
18. V. Lantto, T.T. Rantala, and T.S. Rantala, *J. Eur. Ceram. Soc.* 21, 1961 (2001).
19. C. Malagú, V. Guidi, M. Stefancich, M.C. Carotta, and G. Martinelli, *J. Appl. Phys.* 91, 808 (2002).
20. M.A. Ponce, M.S. Castro, and C.M. Aldao, *Mater. Sci. Eng. B* 111, 14 (2004).
21. N. Barsan, D. Koziej, and U. Weimar, *Sensors Actuators B Chem.* 121, 18 (2007).
22. N. Yamazoe and K. Shimanoe, *Sensors Actuators B Chem.* 138, 100 (2009).
23. A. Giberti, M.C. Carotta, C. Malagú, C.M. Aldao, M.S. Castro, M.A. Ponce, and R. Parra, *Phys. Status Solidi A* 208, 118 (2010).
24. V. Snejdar and J. Jerhot, *Thin Solid Films* 37, 303 (1976).
25. G. Korotcenkov, *Mater. Sci. Eng. B* 139, 1 (2007).
26. C. Altavilla and E. Ciliberto, eds., *Inorganic Nanoparticles: Synthesis, Applications and Perspectives*, chap. 4 (Boca Raton: CRC Press, Taylos & Francis, 2011), pp 69–107.
27. A. Jones, T.A. Jones, B. Mann, and J.G. Firth, *Sensors Actuators B Chem.* 5, 75 (1984).
28. M.J. Willett, V.N. Burganos, C.D. Tsakiroglou, and A.C. Payatakes, *Sensors Actuators B Chem.* 53, 76 (1998).
29. J.P. Ahn, J.H. Kim, J.K. Park, and M.Y. Huh, *Sensors Actuators B Chem.* 99, 18 (2004).
30. M.N. Rahaman, *Ceramic Processing*, chap. 4 and 7 (Boca Raton: CRC Press, Taylor & Francis, 2007), pp. 279–336.
31. P. Boch and J.Cl. Niépce, *Ceramic Materials: Processes, Properties and Applications*, chap. 5 (London: ISTE, 2007), pp. 123–197.
32. R.M. German, *Sintering Theory and Practice* (New York: Wiley, 1996).
33. R.H.R. Castro and K. van Benthem, eds., *Sintering: Mechanisms of Convention Nanodensification and Field Assisted Processes* (Berlin: Engineering Materials Springer Verlag, 2013).
34. C. Ararat, A. Mosquera, R. Parra, M.S. Castro, and J.E. Rodriguez-Paéz, *Mater. Chem. Phys.* 101, 433 (2007).
35. A. Ortiz, M. Mendoza, and J.E. Rodríguez-Páez, *Mater. Res.* 4, 265 (2001).
36. C.E. Ararat, A. Montenegro, and J.E. Rodríguez-Páez, *Quim. Nova* 30, 1578 (2007).
37. D. Amalric-Popescu and F. Bozon-Verduraz, *Catal. Today* 70, 139 (2010).
38. P. Serrini and V. Briois, *Thin Solid Films* 304, 13 (1997).
39. M. Graf, A. Gurlo, N. Barsan, U. Weimar, and A. Hierlemann. *J. Nanopart. Res.* 8, 823 (2006).
40. R. Metz, D. Koumeir, J. Morel, J. Pansiot, M. Houabes, and M. Hassanzadeh, *J. Eur. Ceram. Soc.* 28, 829 (2008).
41. J.A. Cerri, E.R. Leite, D. Gouvea, E. Longo, and J.A. Varela, *J. Am. Ceram. Soc.* 74, 799 (1996).
42. G. Blatter and F. Greuter, *Polycrystalline Semiconductors: Physical Properties and Applications. Springer Series in Solid-State Sciences*, vol. 57, ed. G. Harbeke (Berlin: Springer-Verlag, 1985), pp. 118–137.
43. G. Blatter and F. Greuter, *Phys. Rev. B* 34, 8555 (1986).
44. A.K. Jonscher, *J. Phys. D Appl. Phys.* 32, R57 (1999).
45. D. Khol, *Sensors Actuators B Chem.* 18, 71 (1989).
46. J.C. Phillips and G. Lucovsky, *Bonds and Bands in Semiconductors*, 2nd ed. (New York: Momentum, 2010).
47. F. Greuter, *Solid State Ionics* 75, 67 (1995).
48. A. Broniatowski, *Polycrystalline Semiconductors: Physical Properties and Applications. Springer Series in Solid-State Sciences*, vol. 57, ed. G. Harbeke (Berlin: Springer-Verlag, 1985), pp. 95–117.
49. F. Greuter and G. Blatter, *Semicond. Sci. Technol.* 5, 111 (1990).
50. G.E. Pike, *Grain Boundaries in Semiconductors*, ed. H.J. Leamy, G.E. Pike, and C.H. Seager (London: Elsevier Science, 1982), pp. 369–379.
51. G.E. Pike, *Phys. Rev. B* 30, 795 (1984).